Temperature and density effects on the two-nucleon momentum correlation function from excited single nuclei

Ting-Ting Wang (王婷婷),[1] Yu-Gang Ma (马余刚),[1,2,*] De-Qing Fang (方德清),[1,2] and Huan-Ling Liu (刘焕玲)[3]

[1]*Key Laboratory of Nuclear Physics and Ion-Beam Application (MOE), Institute of Modern Physics, Fudan University, Shanghai 200433, China*

[2]*Shanghai Research Center for Theoretical Nuclear Physics NSFC and Fudan University, Shanghai 200438, China*

[3]*Shanghai Institute of Applied Physics, Chinese Academy of Sciences, Shanghai 201800, China*

(Received 9 January 2022; accepted 11 February 2022; published 28 February 2022)

Two-nucleon momentum correlation functions are investigated for different single thermal sources at given initial temperature (T) and density (ρ). To this end, the space-time evolutions of various single excited nuclei at T = 1–20 MeV and $\rho = 0.2-1.2\ \rho_0$ are simulated by using the thermal isospin-dependent quantum molecular dynamics model. Momentum correlation functions of identical proton-pairs [$C_{pp}(q)$] or neutron-pairs [$C_{nn}(q)$] at small relative momenta are calculated by Lednický and Lyuboshitz analytical method. The results illustrate that $C_{pp}(q)$ and $C_{nn}(q)$ are sensitive to the source size (A) at lower T or higher ρ, but almost not at higher T or lower ρ. And the sensitivities become stronger for smaller source. Moreover, the T, ρ, and A dependencies of the Gaussian source radii are also extracted by fitting the two-proton momentum correlation functions, and the results are consistent with the above conclusions.

DOI: 10.1103/PhysRevC.105.024620

I. INTRODUCTION

Properties of nuclear matter is one of the most interesting topics in heavy-ion physics [1–4] and lots of works have been done around zero temperature, including the nuclear equation of state (EOS). However, the studies on properties of nuclear matter at finite temperatures are relatively limited. Many previous works mainly focus on the temperature dependence of hot nuclear matter and the nuclear liquid-gas phase transition (LGPT) [5–14], the ratio between shear viscosity over entropy density (η/s) [15–19], as well as the nuclear giant dipole resonance [20–22], etc. Among the above works, the relationship between the phase transition temperature and the source size has been investigated [5]. In Ref. [5], the finite-size scaling effects on nuclear liquid-gas phase transition probes are investigated by studying de-excitation processes of the thermal sources by the isospin-dependent quantum molecular dynamics model (IQMD). Several probes, including the total multiplicity derivative, second moment parameter, intermediate mass fragment multiplicity, Fisher's power-law exponent as well as nuclear Zipf's law exponent of Ma [9] were explored, and the phase transition temperatures were then obtained. Recently, the deep neural network has also been used to determine the nuclear liquid gas phase transition [23] and to estimate the temperature of excited nuclei by the charge multiplicity distribution of emitted fragments [24]. The latter work proposed that the charge multiplicity distribution can be used as a thermometer of heavy-ion collisions.

Considering that the intermediate state at high temperature and density in the evolution process of nuclear reactions cannot be directly measured, one always explores properties of nuclear matter and the dynamical description of heavy-ion collisions through the analysis of the final-state products. As is well known, the two-particle momentum correlation function in the final state has been extensively used as a probe of the space-time properties and characteristics of the emission source [25–27]. The two-proton momentum correlation function has been explored systematically by a lot of experiments as well as different models, several reviews can be found in Refs. [28–31]. In various studies on the momentum correlation function, impacts of the impact parameter, the total momentum of nucleon pairs, the isospin of the emission source, the nuclear symmetry energy, the nuclear equation of state (EOS) as well as the in-medium nucleon-nucleon cross section have been discussed in literature [32–38]. Even more, nuclear structure effects were also carefully investigated, such as the effects from binding energy and separation energy of the nucleus [39], density distribution of valence neutrons in neutron-rich nuclei [40], as well as high momentum tail of the nucleon-momentum distribution [41], etc. Two-proton momentum correlation function was also constructed in few-body reactions as well as α-clustered nucleus induced collisions [42–46]. In addition, a momentum correlation function between two light charged particles also offers a unique tool to investigate dynamical expansion of the reaction zone [38].

Here, we extend the momentum correlation method of the final-state interaction to study the time-spatial information of the finite-temperature nuclear systems which have different initial density. The purpose of the present paper is to

*Corresponding author: mayugang@fudan.edu.cn

systematically investigate the relationship between two-particle momentum correlation functions and system parameters, such as the source temperature, density as well as system size in a framework of the thermal isospin-dependent quantum molecular dynamics (ThIQMD) model [5,14,17]. In addition, the Gaussian source radii are quantitatively extracted by an assumption of Gaussian source fits to the momentum correlation function distributions. In this article, the evolution process of excited nuclear sources at given initial temperatures varying from 1 MeV to 20 MeV are studied. The present work selects six different nuclear systems with a similar ratio of neutron to proton numbers, i.e., $N/Z \sim 1.3$, which include $(A, Z) = (36, 15)$, $(52, 24)$, $(80, 33)$, $(100, 45)$, $(112, 50)$, and $(129, 54)$ nuclei. Then, Lednický-Lyuboshitz theoretical approach [47] is applied for calculating two-particle momentum correlation functions which are constructed based on phase-space information from the evolution process of single excited nuclear sources by the ThIQMD model.

The rest of this article is organized as follows. In Sec. II, we first describe the thermal isospin-dependent quantum molecular dynamics model [14,17], then briefly introduce the momentum correlation technique using Lednický and Lyuboshitz (LL) analytical formalism. In Sec. III, we show the results of the ThIQMD plus the LL method for the source-temperature dependence of two-particle momentum correlation function. The two-particle momentum correlation functions of different system sizes at different initial densities are systematically discussed. The detailed analysis of the extracted Gaussian source radii are presented under different source temperature and density. Furthermore, the momentum correlation function of two-neutron is also analyzed. Finally, Sec. IV gives a summary of the paper.

II. MODELS AND FORMALISM

A. The ThIQMD model

In this paper, the thermal isospin-dependent quantum molecular dynamics transport model is used as the event generator, which has been applied successfully to study the LGPT [5,24]. In the following discussion, we introduce this model briefly. As is well-known, the isospin-dependent quantum molecular dynamics (IQMD) model was used to describe the collision process between two nuclei. The quantum molecular dynamics transport model is an n-body transport theory, which describes heavy-ion reaction dynamics from intermediate to relativistic energies [48–51]. In the present work, we use a single excited source in the ThIQMD which is different from the traditional IQMD. Usually, the ground state of the initial nucleus is considered to be $T = 0$ MeV in the traditional IQMD model. However, the ThIQMD model developed by Fang, Ma, and Zhou in Ref. [17] is used to simulate single thermal source at different temperatures and densities.

The main parts of the QMD transport model include the following issues: the initialization of the projectile and the target, nucleon propagation under the effective potential, the collisions between the nucleons in the nuclear medium, and the Pauli blocking effect. In the ThIQMD, instead of using the Fermi-Dirac distribution for $T = 0$ MeV with the nucleon's maximum momentum limited by $P_F^i(\vec{r}) = \hbar[3\pi^2\rho_i(\vec{r})]^{1/3}$, the initial momentum of nucleons is sampled by the Fermi-Dirac distribution at finite temperature:

$$n(e_k) = \frac{g(e_k)}{e^{\frac{e_k-\mu_i}{T}}+1}, \tag{1}$$

where the kinetic energy $e_k = \frac{p^2}{2m}$, p and m are the momentum and mass of the nucleon, respectively. $g(e_k) = \frac{V}{2\pi^2}(\frac{2m}{\hbar^2})^{\frac{3}{2}}\sqrt{e_k}$ represents the state density with the volume of the source $V = \frac{4}{3}\pi r^3$, where $r = r_V A^{\frac{1}{3}}$ (r_V is a parameter to adjust the initial density).

In addition, the chemical potential μ_i is determined by the following equation:

$$\frac{1}{2\pi^2}\left(\frac{2m}{\hbar^2}\right)^{\frac{3}{2}}\int_0^\infty \frac{\sqrt{e_k}}{e^{\frac{e_k-\mu_i}{T}}+1}de_k = \rho_i, \tag{2}$$

where $i = n$ or p refer to the neutron or proton.

In the ThIQMD model, the interaction potential is also represented by the form as follows:

$$U = U_{\rm Sky} + U_{\rm Coul} + U_{\rm Yuk} + U_{\rm Sym} + U_{\rm MDI}, \tag{3}$$

where $U_{\rm Sky}$, $U_{\rm Coul}$, $U_{\rm Yuk}$, $U_{\rm Sym}$, and $U_{\rm MDI}$ are the density-dependent Skyrme potential, the Coulomb potential, the surface Yukawa potential, the isospin asymmetry potential, and the momentum-dependent interaction, respectively. Among these potentials, the Skyrme potential, the Coulomb potential, and the momentum-dependent interaction can be written as

$$U_{\rm Sky} = \alpha\left(\frac{\rho}{\rho_0}\right) + \beta\left(\frac{\rho}{\rho_0}\right)^\gamma, \tag{4}$$

where ρ and ρ_0 are total nucleon density and its normal value at the ground state, i.e., 0.16 fm^{-3}, respectively. The above parameters α, β, and γ with an incompressibility parameter K are related to the nuclear equation of state [52–58]:

$$U_{\rm Sym} = C_{\rm sym}\frac{(\rho_n - \rho_p)}{\rho_0}\tau_z, \tag{5}$$

$$U_{\rm Coul} = \frac{1}{2}(1 - \tau_z)V_c, \tag{6}$$

where ρ_n and ρ_p are neutron and proton densities, respectively, τ_z is the zth component of the isospin degree of freedom for the nucleon, which equals 1 or -1 for a neutron or proton, respectively, and $C_{\rm sym}$ is the symmetry energy coefficient. $U_{\rm Coul}$ is the Coulomb potential where V_c is its parameter for protons:

$$U_{\rm MDI} = \delta\ln^2(\epsilon(\Delta p)^2 + 1)\frac{\rho}{\rho_0}, \tag{7}$$

where Δp is the relative momentum, δ and ϵ can be found in Refs. [48,49]. Their values of the above potential parameters are all listed in Table I.

B. Lednický and Lyuboshitz analytical formalism

Next, we briefly review the method for the two-particle momentum correlation function proposed by Lednický and

TABLE I. The value of the interaction potential parameters.

α (MeV)	β (MeV)	γ	K (MeV)	δ (MeV)	ϵ ((GeV/c)$^{-2}$)
−390.1	320.3	1.14	200	1.57	500

Lyuboshitz [47,59,60]. The momentum correlation technique in nuclear collisions is based on the principle as follows: when they are emitted at small relative momentum, the two-particle momentum correlation is determined by the space-time characteristics of the production processes owing to the effects of quantum statistics (QS) and final-state interactions (FSI) [61,62]. Therefore, the two-particle momentum correlation function can be expressed through a square of the symmetrized Bethe-Salpeter amplitude averaging over the four coordinates of the emitted particles and the total spin of the two-particle system, which represents the continuous spectrum of the two-particle state.

In this theoretical approach, the final-state interactions of the particle pairs is assumed independent in the production process. According to the conditions in Ref. [63], the correlation function of two particles can be written as the expression

$$\mathbf{C}(\mathbf{k}^*) = \frac{\int \mathbf{S}(\mathbf{r}^*, \mathbf{k}^*)|\Psi_{\mathbf{k}^*}(\mathbf{r}^*)|^2 d^4\mathbf{r}^*}{\int \mathbf{S}(\mathbf{r}^*, \mathbf{k}^*) d^4\mathbf{r}^*}, \tag{8}$$

where $\mathbf{r}^* = \mathbf{x}_1 - \mathbf{x}_2$ is the relative distance of the two particles in the pair rest frame (PRF) at their kinetic freeze-out, $\mathbf{k}^*$ is half of the relative momentum between two particles in the PRF, $\mathbf{S}(\mathbf{r}^*, \mathbf{k}^*)$ is the probability to emit a particle pair with given $\mathbf{r}^*$ and $\mathbf{k}^*$, i.e., the source emission function, and $\Psi_{\mathbf{k}^*}(\mathbf{r}^*)$ is the equal-time ($t^* = 0$) reduced Bethe-Salpeter amplitude which can be approximated by the outer solution of the scattering problem in the PRF [64,65]. This approximation is valid on condition $|t^*| \ll m(r^*)^2$, which is well fulfilled for sufficiently heavy particles like protons or kaons and reasonably fulfilled even for pions [59]. In the above limit, the asymptotic solution of the wave function of the two charged particles approximately takes the expression

$$\Psi_{\mathbf{k}^*}(\mathbf{r}^*) = e^{i\delta_c}\sqrt{A_c(\lambda)} \times\left[e^{-i\mathbf{k}^*\mathbf{r}^*}F(-i\lambda, 1, i\xi) + f_c(k^*)\frac{\tilde{G}(\rho, \lambda)}{r^*}\right]. \tag{9}$$

In the above equation, $\delta_c =$ arg $\Gamma(1 + i\lambda)$ is the Coulomb s-wave phase shift with $\lambda = (k^* a_c)^{-1}$, where a_c is the two-particle Bohr radius, $A_c(\lambda) = 2\pi\lambda[\exp(2\pi\lambda) - 1]^{-1}$ is the Coulomb penetration factor, and its positive (negative) value corresponds to the repulsion (attraction). $\tilde{G}(\rho, \lambda) = \sqrt{A_c(\lambda)}[G_0(\rho, \lambda) + iF_0(\rho, \lambda)]$ is a combination of regular (F_0) and singular (G_0) s-wave Coulomb functions [59,60]. $F(-i\lambda, 1, i\xi) = 1 + (-i\lambda)(i\xi)/1!^2 + (-i\lambda)(-i\lambda + 1)(i\xi)^2/2!^2 + \cdots$ is the confluent hypergeometric function with $\xi = \mathbf{k}^*\mathbf{r}^* + \rho$, $\rho = k^* r^*$:

$$f_c(k^*) = \left[K_c(k^*) - \frac{2}{a_c}h(\lambda) - ik^* A_c(\lambda)\right]^{-1} \tag{10}$$

is the s-wave scattering amplitude renormalized by the long-range Coulomb interaction with $h(\lambda) = \lambda^2\sum_{n=1}^{\infty}[n(n^2 + \lambda^2)]^{-1} - C - \ln[\lambda]$, where $C = 0.5772$ is the Euler constant. $K_c(k^*) = \frac{1}{f_0} + \frac{1}{2}d_0 k^{*2} + Pk^{*4} + \cdots$ is the effective range function, where d_0 is the effective radius of the strong interaction, f_0 is the scattering length, and P is the shape parameter. The parameters of the effective range function are important parameters characterizing the essential properties of the FSI, and can be extracted from the correlation function measured experimentally [38,65–67].

For n-n momentum correlation functions which include an uncharged particle, only the short-range particle interaction works. For p-p momentum correlation functions, both the Coulomb interaction and the short-range particle interaction dominated by the s-wave interaction are taken into account.

III. ANALYSIS AND DISCUSSION

Within the framework of the thermal isospin-dependent quantum molecular dynamics model [5,14,17], the two-particle momentum correlation functions are calculated by using the phase-space information from the freeze-out stage of the excited nuclear source at an initial temperature varying from 1 MeV to 20 MeV and/or density varying

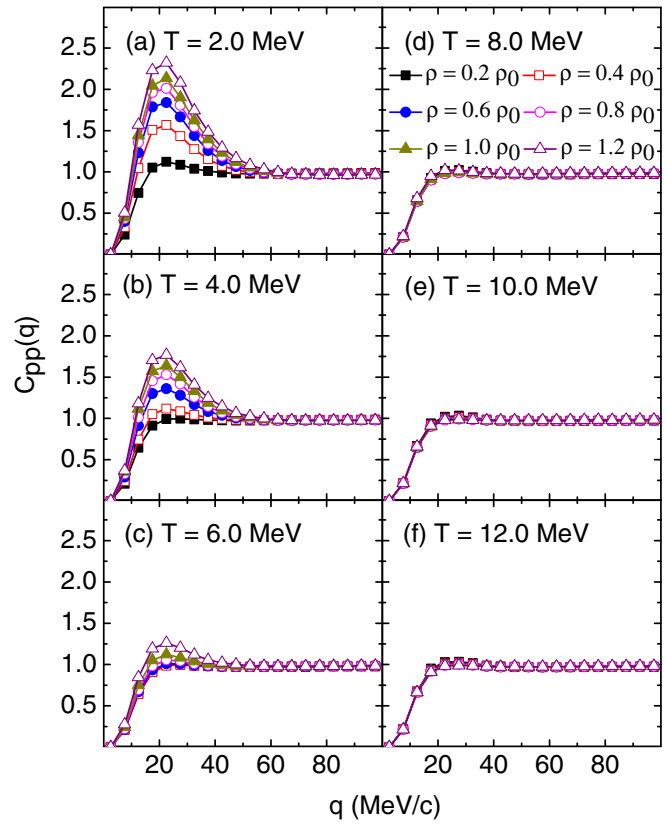

FIG. 1. The proton-proton momentum correlation function [$C_{pp}(q)$] at different densities (i.e., $0.2\rho_0$, $0.4\rho_0$, $0.6\rho_0$, $0.8\rho_0$, $1.0\rho_0$, and $1.2\rho_0$) for the smaller nucleus ($A = 36$, $Z = 15$) with fixed source-temperatures $T = 2$ MeV (a), 4 MeV (b), 6 MeV (c), 8 MeV (d), 10 MeV (e), and 12 MeV (f), respectively. The freeze-out time is taken to be 200 fm/c.

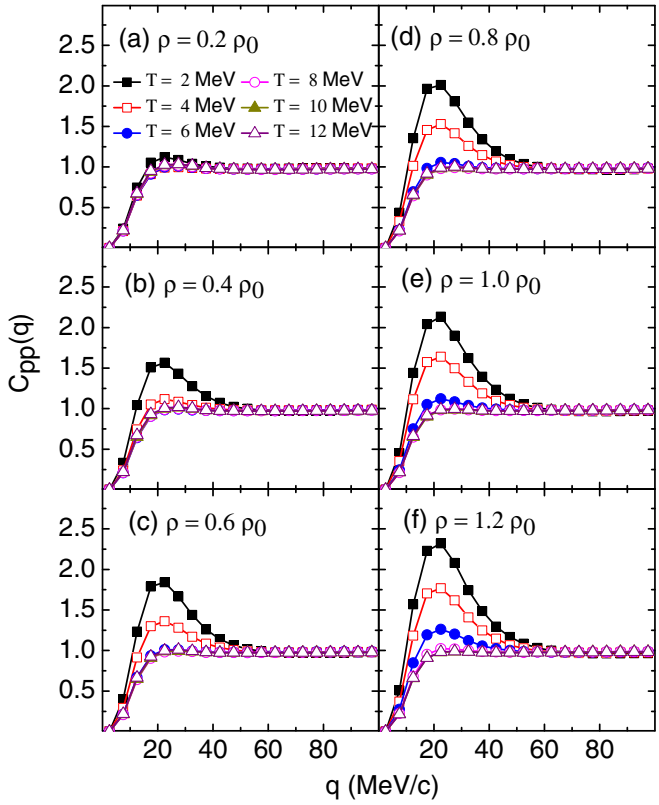

FIG. 2. Similar to Fig. 1, but at different source-temperatures (T = 2, 4, 6, 8, 10, and 12 MeV) with different fixed densities, namely $\rho = 0.2\rho_0$ (a), 0.4 ρ_0 (b), 0.6 ρ_0 (c), 0.8 ρ_0 (d), 1.0 ρ_0 (e), and 1.2ρ_0 (f).

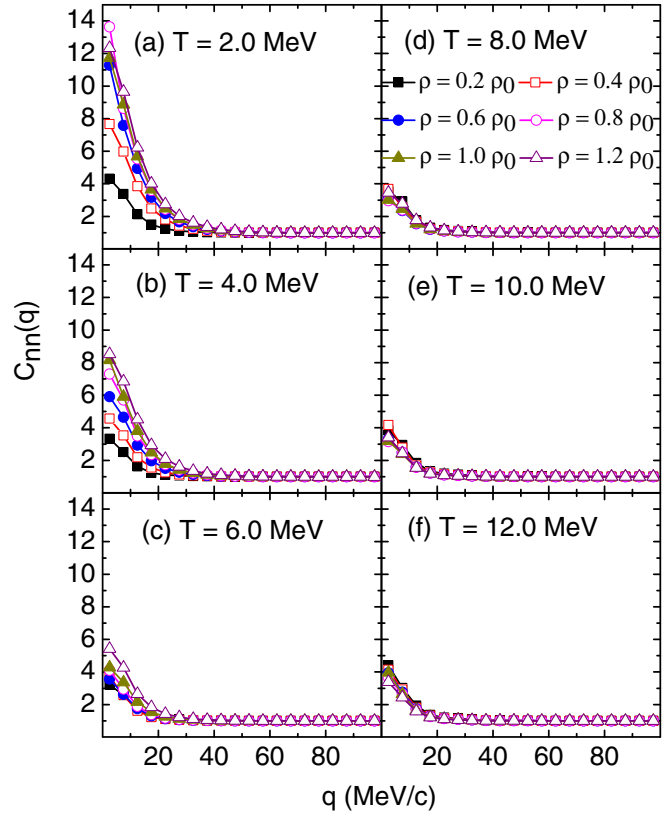

FIG. 3. The neutron-neutron (n-n) momentum correlation functions [$C_{nn}(q)$] in the same conditions as Fig. 1.

from $\rho = 0.2\rho_0$ to $1.2\rho_0$. This work performs calculations for thermal source systems with different mass including $(A, Z) = (36, 15)$, $(52, 24)$, $(80, 33)$, $(100, 45)$, $(112, 50)$, and $(129, 54)$.

We first calculated the proton-proton momentum correlation function $C_{pp}(q)$ for finite-size systems at temperatures ranging from 1 to 20 MeV. In Fig. 1, the results of $C_{pp}(q)$ for temperature of 2, 4, 6, 8, 10 and 12 MeV at different values of density ($0.2\rho_0$ - $1.2\rho_0$) are presented. The proton-proton momentum correlation function exhibits a peak at relative momentum $q = 20$ MeV/c, which is due to the strong final-state s-wave attraction together with the suppression at lower relative momentum as a result of Coulomb repulsion and the antisymmetrization wave function between two protons. The shape of the two-proton momentum correlation functions is consistent with many previous experimental data in heavy-ion collisions, e.g., Ref. [68]. For protons which are emitted from the lower temperature ($T < 8$ MeV) source in Fig. 1(a)–1(c), the general trend is very similar. The figure shows that $C_{pp}(q)$ increases as ρ increases for fixed T ($T < 8$ MeV). The increase of the density indicates that the geometrical size becomes smaller for a source with fixed neutrons and protons, which makes the strength of the momentum correlation function stronger. Finally, the p-p momentum correlation function becomes almost one at $q > 60$ MeV/c. For larger T ($T > 8$ MeV) in Fig. 1(d)–1(f), the difference of $C_{pp}(q)$

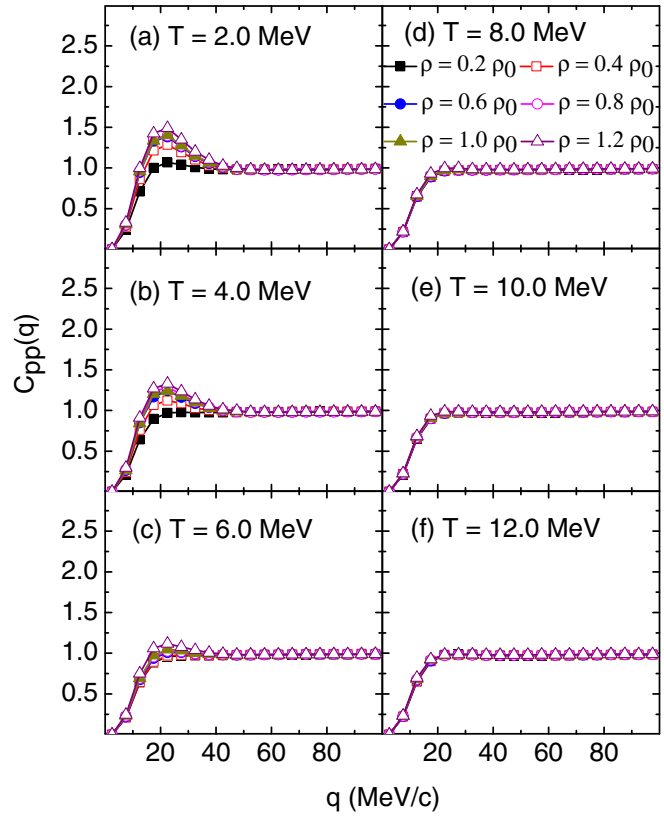

FIG. 4. Same to Fig. 1, but for a larger system ($A = 129$, $Z = 54$).

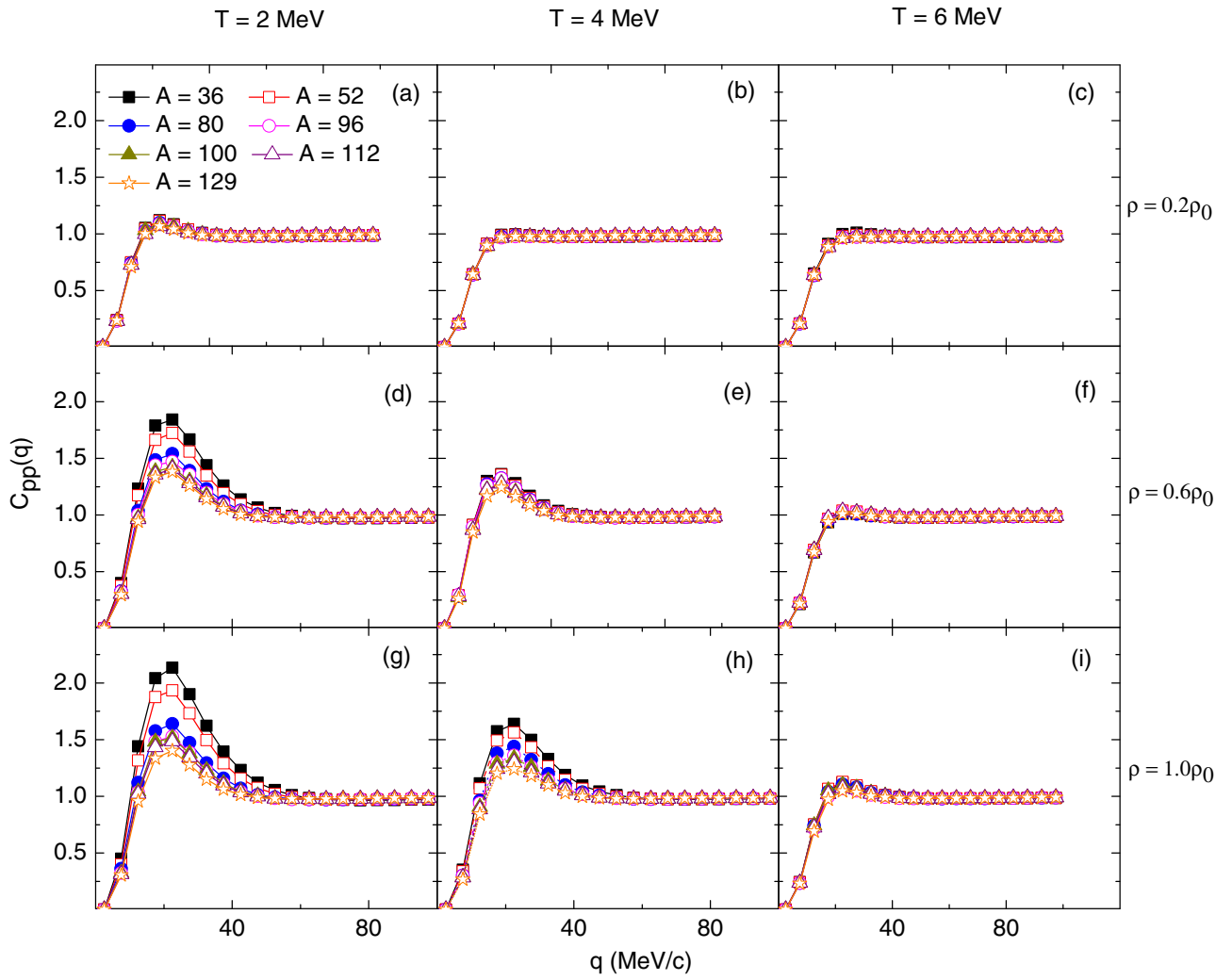

FIG. 5. $C_{pp}(q)$ of different source size systems at fixed temperatures (i.e., from left column to right column, they correspond to $T = 2$, 4, and 6 MeV, respectively) or fixed densities (i.e., from top row to bottom row, they correspond to $\rho = 0.2\rho_0$, $0.6\rho_0$, $1.0\rho_0$, respectively).

between different densities becomes smaller. From Fig. 1, it is found that the $C_{pp}(q)$ almost keep the same above $T = 8$ MeV for different densities and the p-p momentum correlation function becomes almost unique above approximately $q = 30$ MeV/c. It indicates that the emitted proton is not affected by the change of density when the source temperature beyond certain value ($T \approx 8$ MeV in present work). In order to understand which one of the two factors (i.e., temperature and density) has larger influence, the two-particle momentum correlation in Fig. 2 is plotted by exchanging of the two input parameters. From Fig. 2, we can intuitively observe dependence of the two-particle momentum correlation on the source temperature. The dependence of $C_{pp}(q)$ on the source temperature is stronger than on density. In other words, the $C_{pp}(q)$ is more sensitive to T than to density ρ. In addition, for larger ρ from Fig. 2(a) to (f), the difference of $C_{pp}(q)$ between different densities becomes bigger. Next, we explore whether the phenomenon exists in momentum correlation functions for the uncharged-particle pairs. Figure 3 presents the neutron-neutron momentum correlation functions [$C_{nn}(q)$] for temperature of 2, 4, 6, 8, 10, and 12 MeV at different values of density, respectively. For neutron-neutron momentum correlation function, it peaks at $q \approx 0$ MeV/c caused by the s-wave attraction. Although the $C_{nn}(q)$ has different shape compared with the p-p momentum correlation function, it has the similar dependence on the source temperature and density. The similar trend in $C_{pp}(q)$ and $C_{nn}(q)$ shows the close emission mechanism in the evolution process.

Figure 4 shows the results of a larger system at different source-temperature and density, and a similar behavior of $C_{pp}(q)$ is demonstrated. We also observe that the proton-proton momentum correlation in larger-size system [$(A, Z) = (129, 54)$] in Fig. 4 becomes weaker in comparison with the smaller-size source [$(A, Z) = (36, 15)$] in Fig. 1. In view of the above phenomenon, Fig. 5 describes the relationship between system-size and momentum correlation function in more details. The decreasing of $C_{pp}(q)$ as the system-size increasing for a fixed value of T or ρ can be clearly seen in Fig. 5(g), which is consistent with the previous results of Gaussian source [37,38,69]. In Fig. 5(a)–5(i), with larger temperature or lower density, the difference of $C_{pp}(q)$ between different T or ρ becomes smaller, respectively. The Gaussian

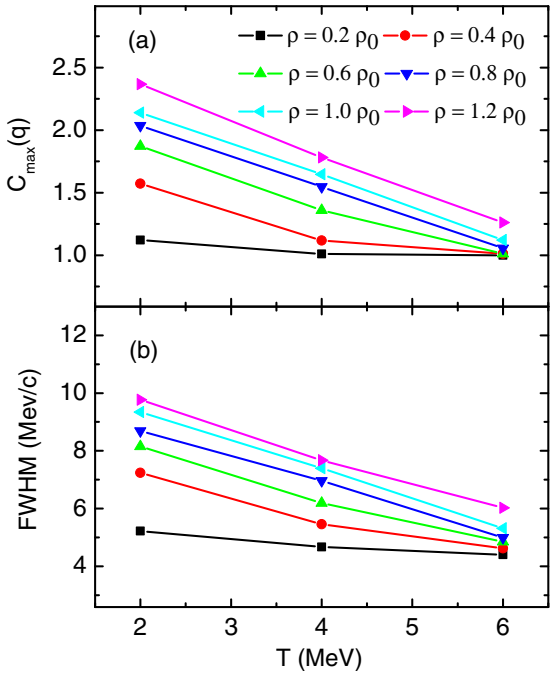

FIG. 6. Source-temperature T dependencies of $C_{\max}(q)$ (a) and of FWHM (b) of $C_{pp}(q)$ distributions at different densities ($0.2\rho_0$–$1.2\rho_0$) for the ($A = 35, Z = 16$) system.

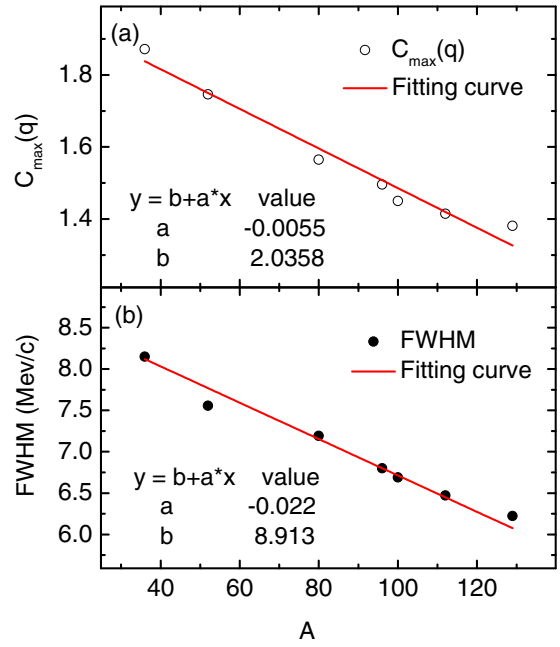

FIG. 7. $C_{\max}(q)$ (a) and FWHM (b) for different source-size systems at given $T = 2$ MeV and $\rho = 0.6\rho_0$.

source radii are extracted for further discussion later in this article.

From the above plots, we can extract $C_{\max}(q)$, i.e., the maximum value of $C_{pp}(q)$ as well as the full width at half-maximum (FWHM) of $C_{pp}(q)$ distribution, i.e., at $C_{pp}(q) = [C_{\max}(q) - 1]/2$. The source-temperature T dependence of $C_{\max}(q)$ and FWHM for the proton-proton momentum correlation function with different density are given in Fig. 6. As shown in Fig. 6(a) and 6(b), both $C_{\max}(q)$ and FWHM decrease gradually with the increasing of T. In addition, both of them increase gradually with density. At high temperature, the change of $C_{\max}(q)$ and FWHM is very small and not plotted in the figure. Of course, the behavior of the $C_{\max}(q)$ and FWHM with T and ρ can also be clearly seen in Fig. 2, and the increasing of $C_{\max}(q)$ and FWHM are generally inversely proportional to Gaussian radius r_0 as shown later. Similarly, the system-size A dependence of $C_{\max}(q)$ and FWHM for the proton-proton momentum correlation function at $T = 2$ MeV and $\rho = 0.6\rho_0$ is shown in Fig. 7. The dependence of $C_{\max}(q)$ and FWHM on system-size A is quite similar to the temperature dependence in Fig. 6. The $C_{\max}(q)$ and FWHM values become smaller for larger systems.

Figure 8 shows the source-temperature, density, and system-size dependence of Gaussian radii extracted from two-particle momentum correlation functions, where panels (a) and (b) are results with the smaller source size and the larger source size, respectively. The radii are extracted by a Gaussian source assumption, i.e., $S(r) \approx \exp[-r^2/(4r_0^2)]$, where r_0 is the Gaussian source radius from the proton-proton momentum correlation functions. The theoretical calculations for $C_{pp}(q)$ was performed by using the Lednický and Lyuboshitz analytical method. The best fitting radius is judged by finding the minimum of the reduced χ-square between the ThIQMD calculations and the Gaussian source assumption. Since the effect of the strong FSI scales as $f_c(k^*)/r^*$ in Eq. (9), one may read the sensitivity of the correlation function to the temperature T, density ρ, and atomic number A from their

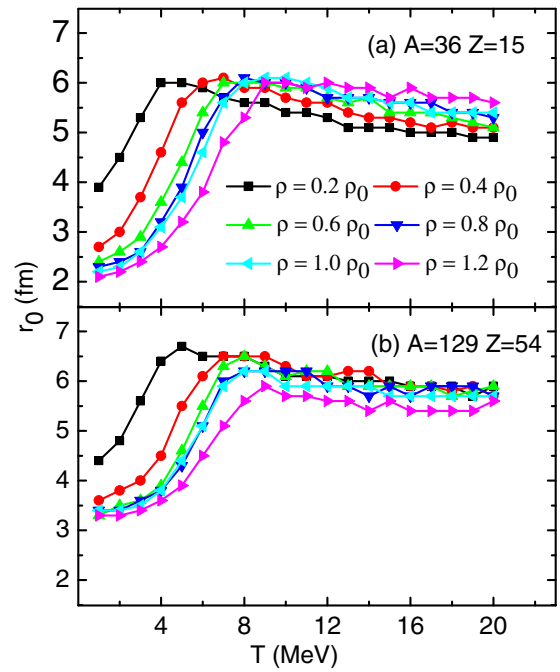

FIG. 8. Gaussian source radius as a function of temperature at different densities ($\rho = 0.2\rho_0, 0.4\rho_0, 0.6\rho_0, 0.8\rho_0, 1.0\rho_0, 1.2\rho_0$) for a fixed source size. (a) and (b) correspond to the smaller source size with ($A = 36, Z = 15$) and the larger source size with ($A = 129, Z = 54$), respectively.

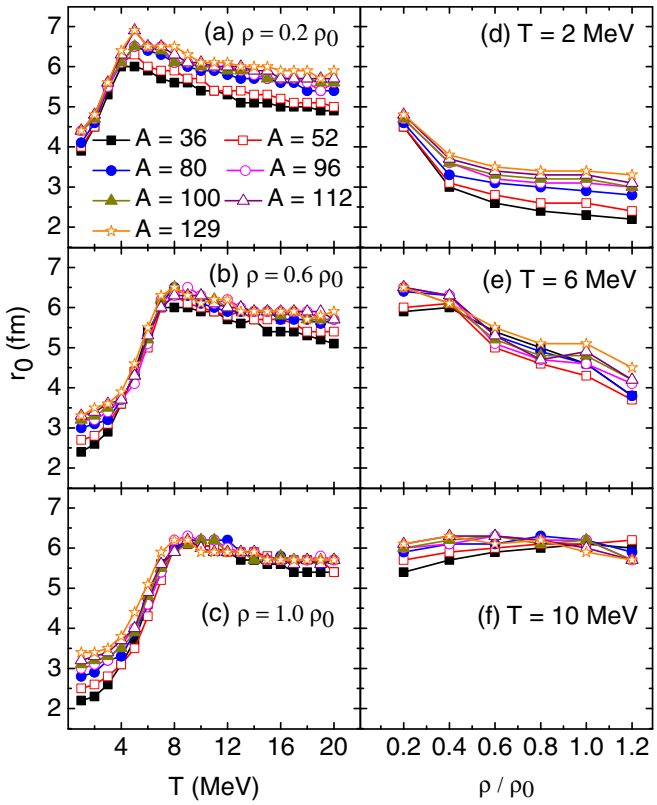

FIG. 9. Gaussian source radius as a function of temperature or density at different source-size systems. Left and right columns correspond to r_0 at different densities, i.e., $\rho = 0.2\ \rho_0$ (a), $0.6\ \rho_0$ (b), and $1.0\ \rho_0$ (c) as well as different temperatures, i.e., $T = 2$ (d), 6 (e), and 10 (f) MeV, respectively.

effects on the Gaussian radius r_0. One may observe a linear dependence on these parameters up to $T \approx 8$ MeV and then a lost of sensitivity in a plateau region at higher temperatures in Fig. 8. As the density decreases, the decreasing speed of the Gaussian radius of the small system is larger than that of the larger system. Figure 9 shows the Gaussian radius of the different system-size varies with the temperature in panels (a)–(c) or density in panels (d)–(f). The Gaussian source radius is consistent with the system-size, i.e., at higher temperature or larger density, the differences of Gaussian source between different system sizes are bigger in the low density and low temperature region, but the difference in opposite conditions almost disappear. In other words, the sensitivity of the source radii to the system size seem to be different in the different regions of temperatures and densities. For example, the sensitivity is better in the region of lower T and higher ρ [Fig. 9(b) and 9(c)], or it is better in the higher T region for the lower ρ [Fig. 9(a)], or it is better in the higher ρ region for the lower T [Fig. 9(d)].

From the above discussion, it is demonstrated that the strength of the two-particle momentum correlation function is affected by the source temperature, density, and system size. The two-particle momentum correlation function strength is larger for a single source with lower temperature, higher density or smaller mass number as shown in Figs. 1–5. Otherwise, the strength becomes smaller. To some extents, the strong correlation between two particles is mainly caused by the closed position of each other in phase space in both coordinate and momentum. Varying only one in the three condition parameters (temperature, density, and system size), lower temperature means smaller momentum space, higher density means smaller coordinate space, and small system size also mean smaller coordinate space to keep fixed density compared with large system size. The dependencies of the two-particle momentum correlation function strength on the source temperature, density, and system size could be explained by the change of the phase space sizes. Two particles emitted from small phase space will have strong correlation and those from large phase space will have weak correlation. For example, the increase of the $C_{pp}(q)$ strength with the increase of the density for a fixed system size could be explained by the decreasing of the coordinate space as shown in Fig. 1(a). And the small $C_{pp}(q)$ strength at temperature higher than 8 MeV could be caused by the large momentum space compared with lower temperatures as shown in Fig. 1(d)–1(f). The decrease of the $C_{pp}(q)$ strength with the increase of the system size for a fixed density could also be explained by the increasing of the coordinate space as shown in Fig. 5(g). Thus it is concluded that the phase space size for the emitted nucleons have strong effect on strength of the two-particle momentum correlation function, which can also be seen in the extracted Gaussian radii as shown in Fig. 8.

IV. SUMMARY

In summary, the two-particle momentum correlation functions for single excited sources are investigated using the Lednický and Lyuboshitz analytical formalism with the phase-space information at the freeze-out stage for different initial temperatures and densities in a framework of the ThIQMD transport approach. We mainly performed a series of studies focusing on the varied effects of source temperature, density, and system-size on the two-particle momentum correlation functions. The results reflect that the shape of the two-proton momentum correlation function is in accordance with the previous experimental data in heavy-ion collisions [68]. At the same time, the trend of the relationship between the two-proton momentum correlation and system-size is consistent with previous simulations [37,38,69]. At low source temperature, the larger density makes the two-particle momentum correlation stronger. However, at higher source temperature, the effect almost disappear. Both proton-proton correlations and neutron-neutron correlations have the similar responses to temperature and density. This work also shows that the emission source is not much influenced by density above a certain temperature for a single excited source. In the same way, the emission source is softly influenced by temperature below a given density for a single excited source. In one word, the dependence of the two-particle momentum correlation function on the source temperature, density, and system size could be explained by the change of the coordinate and/or momentum phase space sizes. In the end, the Gaussian radii are extracted to explore the emission source sizes in single excited systems. Gaussian radii become larger in the larger systems. The dependence of the extracted Gaussian radius on

source-temperature and density is consistent with behavior of the two-proton momentum correlation function as discussed in the texts.

ACKNOWLEDGMENTS

This work was supported in part by the National Natural Science Foundation of China under Contracts No. 11890710, No. 11890714, No. 11875066, No. 11925502, No. 11961141003, No. 11935001, No. 12147101, and No. 12047514, the Strategic Priority Research Program of CAS under Grant No. XDB34000000, National Key R&D Program of China under Grants No. 2016YFE0100900 and No. 2018YFE0104600, Guangdong Major Project of Basic and Applied Basic Research No. 2020B0301030008, and the China PostDoctoral Science Foundation under Grant No. 2020M681140.

[1] G. Giuliani, H. Zheng, and A. Bonasera, Prog. Part. Nucl. Phys. **76**, 116 (2014).
[2] B. A. Li, L. W. Chen, and C. M. Ko, Phys. Rep. **464**, 113 (2008).
[3] B. Borderie and M. F. Rivet, Prog. Part. Nucl. Phys. **61**, 551 (2008).
[4] C. W. Ma and Y.-G. Ma, Prog. Part. Nucl. Phys. **99**, 120 (2018).
[5] H. L. Liu, Y. G. Ma, and D. Q. Fang, Phys. Rev. C **99**, 054614 (2019).
[6] J. E. Finn, S. Agarwal, A. Bujak, J. Chuang, L. J. Gutay, A. S. Hirsch, R. W. Minich, N. T. Porile, R. P. Scharenberg, B. C. Stringfellow, and F. Turkot, Phys. Rev. Lett. **49**, 1321 (1982).
[7] P. J. Siemens, Nature **305**, 410 (1983).
[8] Y. G. Ma, A. Siwek, J. Péter *et al.*, Phys. Lett. B **390**, 41 (1997).
[9] Y. G. Ma, Phys. Rev. Lett. **83**, 3617 (1999).
[10] P. Chomaz, V. Duflot, and F. Gulminelli, Phys. Rev. Lett. **85**, 3587 (2000).
[11] J. B. Natowitz, K. Hagel, Y. G. Ma, M. Murray, L. Qin, R. Wada, and J. Wang, Phys. Rev. Lett. **89**, 212701 (2002).
[12] Y. G. Ma, J. B. Natowitz, R. Wada, K. Hagel, J. Wang, T. Keutgen, Z. Majka, M. Murray, L. Qin, P. Smith, R. Alfaro, J. Cibor, M. Cinausero, Y. El Masri, D. Fabris, E. Fioretto, A. Keksis, M. Lunardon, A. Makeev, N. Marie, E. Martin, A. Martinez-Davalos, A. Menchaca-Rocha, G. Nebbia, G. Prete, V. Rizzi, A. Ruangma, D. V. Shetty, G. Souliotis, P. Staszel, M. Veselsky, G. Viesti, E. M. Winchester, and S. J. Yennello, Phys. Rev. C **71**, 054606 (2005).
[13] B. Borderie and J. Frankland, Prog. Part. Nucl. Phys. **105**, 82 (2019).
[14] Z.-F. Zhang, D.-Q. Fang, and Y.-G. Ma, Nucl. Sci. Tech. **29**, 78 (2018).
[15] N. Auerbach and S. Shlomo, Phys. Rev. Lett. **103**, 172501 (2009).
[16] N. Dinh Dang, Phys. Rev. C **84**, 034309 (2011).
[17] D. Q. Fang, Y. G. Ma, and C. L. Zhou, Phys. Rev. C **89**, 047601 (2014).
[18] X. G. Deng, Y. G. Ma, and M. Veselský, Phys. Rev. C **94**, 044622 (2016).
[19] D. Mondal, D. Pandit, S. Mukhopadhyay, S. Pal, B. Dey, S. Bhattacharya, A. De, S. Bhattacharya, S. Bhattacharyya, P. Roy, K. Banerjee, and S. R. Banerjee, Phys. Rev. Lett. **118**, 192501 (2017).
[20] A. Bracco, J. J. Gaardhøje, A. M. Bruce, J. D. Garrett, B. Herskind, M. Pignanelli, D. Barnéoud, H. Nifenecker, J. A. Pinston, C. Ristori, F. Schussler, J. Bacelar, and H. Hofmann, Phys. Rev. Lett. **62**, 2080 (1989).
[21] P. F. Bortignon, A. Bracco, D. Brink, and R. A. Broglia, Phys. Rev. Lett. **67**, 3360 (1991).
[22] O. Wieland, A. Bracco, F. Camera, G. Benzoni, N. Blasi, S. Brambilla, F. Crespi, A. Giussani, S. Leoni, B. Million, A. Moroni, S. Barlini, V. L. Kravchuk, F. Gramegna, A. Lanchais, P. Mastinu, A. Maj, M. Brekiesz, M. Kmiecik, M. Bruno, E. Geraci, G. Vannini, G. Casini, M. Chiari, A. Nannini, A. Ordine, and E. Ormand, Phys. Rev. Lett. **97**, 012501 (2006).
[23] R. Wang, Y. G. Ma, R. Wada, L. W. Chen, W. B. He, H. L. Liu, and K. J. Sun, Phys. Rev. Research **2**, 043202 (2020).
[24] Y. D. Song, R. Wang, Y. G. Ma, X. G. Deng, and H. L. Liu, Phys. Lett. B **814**, 136084 (2021).
[25] R. Kotte *et al.*, Eur. Phys. J. A **23**, 271 (2005).
[26] R. Ghetti, J. Helgesson, V. Avdeichikov, P. Golubev, B. Jakobsson, N. Colonna, G. Tagliente, S. Kopecky, V. L. Kravchuk, H. W. Wilschut, E. W. Andersson, P. Nadel-Turonski, L. Westerberg, V. Bellini, M. L. Sperduto, and C. Sutera, Phys. Rev. Lett. **91**, 092701 (2003).
[27] D. Gourio *et al.*, Eur. Phys. J. A **7**, 245 (2000).
[28] D. H. Boal, C. K. Gelbke, and B. K. Jennings, Rev. Mod. Phys. **62**, 553 (1990).
[29] U. A. Wiedemann and U. Heinz, Phys. Rep. **319**, 145 (1999).
[30] M. A. Lisa, S. Pratt, R. Soltz, and U. Wiedemann, Annu. Rev. Nucl. Part. Sci. **55**, 357 (2005).
[31] G. Verde, A. Chbihi, R. Ghetti, and J. Helgesson, Eur. Phys. J. A **30**, 81 (2006).
[32] W. G. Gong, W. Bauer, C. K. Gelbke, and S. Pratt, Phys. Rev. C **43**, 781 (1991).
[33] G. Verde, D. A. Brown, P. Danielewicz, C. K. Gelbke, W. G. Lynch, and M. B. Tsang, Phys. Rev. C **65**, 054609 (2002).
[34] Y. G. Ma, Y. B. Wei, W. Q. Shen, X. Z. Cai, J. G. Chen, J. H. Chen, D. Q. Fang, W. Guo, C. W. Ma, G. L. Ma, Q. M. Su, W. D. Tian, K. Wang, T. Z. Yan, C. Zhong, and J. X. Zuo, Phys. Rev. C **73**, 014604 (2006).
[35] R. Ghetti, V. Avdeichikov, B. Jakobsson, P. Golubev, J. Helgesson, N. Colonna, G. Tagliente, H. W. Wilschut, S. Kopecky, V. L. Kravchuk, E. W. Anderson, P. Nadel-Turonski, L. Westerberg, V. Bellini, M. L. Sperduto, and C. Sutera, Phys. Rev. C **69**, 031605(R) (2004).
[36] L. W. Chen, V. Greco, C. M. Ko, and B. A. Li, Phys. Rev. Lett. **90**, 162701 (2003).
[37] T.-T. Wang, Y.-G. Ma, C.-J. Zhang, and Z.-Q. Zhang, Phys. Rev. C **97**, 034617 (2018).
[38] T.-T. Wang, Y.-G. Ma, and Z.-Q. Zhang, Phys. Rev. C **99**, 054626 (2019).
[39] Y. B. Wei *et al.*, Phys. Lett. B **586**, 225 (2004).
[40] X. G. Cao, X. Z. Cai, Y. G. Ma, D. Q. Fang, G. Q. Zhang, W. Guo, J. G. Chen, and J. S. Wang, Phys. Rev. C **86**, 044620 (2012).
[41] G.-F. Wei, X.-G. Cao, Q.-J. Zhi, X.-W. Cao, and Z.-W. Long, Phys. Rev. C **101**, 014613 (2020).

[42] B. S. Huang and Y. G. Ma, Phys. Rev. C **101**, 034615 (2020).
[43] D. Q. Fang, Y. G. Ma, X. Y. Sun, P. Zhou, Y. Togano, N. Aoi, H. Baba, X. Z. Cai, X. G. Cao, J. G. Chen, Y. Fu, W. Guo, Y. Hara, T. Honda, Z. G. Hu, K. Ieki, Y. Ishibashi, Y. Ito, N. Iwasa, S. Kanno, T. Kawabata, H. Kimura, Y. Kondo, K. Kurita, M. Kurokawa, T. Moriguchi, H. Murakami, H. Ooishi, K. Okada, S. Ota, A. Ozawa, H. Sakurai, S. Shimoura, R. Shioda, E. Takeshita, S. Takeuchi, W. D. Tian, H. W. Wang, J. S. Wang, M. Wang, K. Yamada, Y. Yamada, Y. Yasuda, K. Yoneda, G. Q. Zhang, and T. Motobayashi, Phys. Rev. C **94**, 044621 (2016).
[44] B.-S. Huang, Y.-G. Ma, Chin. Phys. C **44**, 094105 (2020).
[45] L. Shen, B. S. Huang, and Y. G. Ma, Phys. Rev. C **105**, 014603 (2022).
[46] J. J. He, S. Zhang, Y. G. Ma, J. H. Chen, and C. Zhong, Eur. Phys. J. A **56**, 52 (2020).
[47] R. Lednický, Nucl. Phys. A **774**, 189 (2006).
[48] J. Aichelin, A. Rosenhauer, G. Peilert, H. Stoecker, and W. Greiner, Phys. Rev. Lett. **58**, 1926 (1987).
[49] J. Aichelin, Phys. Rep. **202**, 233 (1991).
[50] G. Peilert, H. Stöcker, W. Greiner, A. Rosenhauer, A. Bohnet, and J. Aichelin, Phys. Rev. C **39**, 1402 (1989).
[51] Z.-Q. Feng, Nucl. Sci. Tech. **29**, 40 (2018).
[52] Y. G. Ma *et al.*, Nucl. Phys. A **787**, 611 (2007).
[53] J. Liu, C. Gao, N. Wan, and C. Xu, Nucl. Sci. Tech. **32**, 117 (2021).
[54] F. Zhang and J. Su, Nucl. Sci. Tech. **31**, 77 (2020).
[55] H. Yu, D.-Q. Fang, and Y.-G. Ma, Nucl. Sci. Tech. **31**, 61 (2020).
[56] G.-F. Wei, Q.-J. Zhi, X.-W. Cao, and Z.-W. Long, Nucl. Sci. Tech. **31**, 71 (2020).
[57] C.-J. Jiang *et al.*, Chin. Phys. Lett. **38**, 052101 (2021).
[58] J. Xu, Chin. Phys. Lett. **38**, 042101 (2021).
[59] R. Lednický, Phys. Part. Nucl. **40**, 307 (2009).
[60] R. Lednický, Phys. At. Nucl. **71**, 1572 (2008).
[61] S. E. Koonin, Phys. Lett. B **70**, 43 (1977).
[62] R. Lednický, Braz. J. Phys. **37**, 939 (2007).
[63] R. Lednický, V. L. Lyuboshitz, B. Erazmus, and D. Nouais, Phys. Lett. B **373**, 30 (1996).
[64] R. Lednický and V. L. Lyuboshitz, Sov. J. Nucl. Phys. **35**, 770 (1982).
[65] L. Adamczyk *et al.* (STAR Collaboration), Nature **527**, 345 (2015).
[66] B. Erazmus, L. Martin, R. Lednicky, and N. Carjan, Phys. Rev. C **49**, 349 (1994).
[67] J. Arvieux, Nucl. Phys. A **221**, 253 (1974).
[68] R. Ghetti *et al.*, Nucl. Phys. A **674**, 277 (2000).
[69] L. Zhou and D.-Q. Fang, Nucl. Sci. Tech. **31**, 52 (2020).